ELSEVIER

1 May 1995

OPTICS COMMUNICATIONS

Optics Communications 116 (1995) 291–299

Full length article

Polarisation contrast imaging of thin films in scanning microscopy

S.V. Shatalin, J.B. Tan, R. Juškaitis, T. Wilson

Department of Engineering Science, University of Oxford, Parks Road, Oxford, OX1 3PJ, UK

Received 15 July 1994; revised version received 7 November 1994

Abstract

We consider the form of the optical field in the exit pupil of a high numerical aperture microscope objective when the lens is focussed onto an isotropic thin film specimen. The form of the optical field is particularly sensitive to specimen properties and is usually not circularly symmetric. We propose and demonstrate a polarisation difference imaging mode which takes advantage of this asymmetry to provide images of greatly enhanced contrast.

1. Introduction

Ellipsometry is a very powerful technique which is widely used in a variety of disciplines to obtain information about the optical properties of surfaces and thin film structures [1]. The technique consists, in essence, of illuminating the specimen with an obliquely incident plane wave and measuring the change in polarisation state of this wave after reflection. The tremendous sensitivity of this technique suggests that interesting and important contrast should be available in a scanning optical microscope if we image polarisation changes on reflection from the specimen. In a microscope, of course, a high numerical aperture objective lens is used to illuminate the specimen. We can think of the effect of using a lens as illuminating the specimen with an angular spectrum of plane waves and hence the system we will describe may be thought of as a large number of ellipsometers in parallel. The polarisation state of the reflected light in the exit pupil of the objective lens will then depend crucially on the optical properties of the specimen under test.

We will begin by developing theoretical expressions for the polarisation state at the exit pupil of the lens when the objective is focussed onto a planar specimen and present experimental confirmation of these predictions. In this sense our measurements are similar to conventional conoscopy [2] although we are considering both a reflection system and isotropic specimens. We will take advantage of the fact that the field at the exit pupil of the objective lens is not, in general, angularly symmetric to construct a scanning microscope in which image contrast is determined by the polarisation properties of the specimen under examination.

2. Preliminary considerations

In order to proceed further it is necessary to develop an expression for the field at the exit pupil of a high numerical aperture objective lens which has focussed an incident plan polarised beam of light onto a planar specimen. The geometry is shown in Fig. 1. Our approach is to consider a particular component of the angular spectrum of plane waves which is incident on the specimen at an angle, ϕ. We assume that the incident beam is of amplitude E_0 and is polarised in the i_x direction. After refraction by the lens this field may be resolved into both transverse electric (TE), $-E_0 \sin\theta$, and transverse magnetic (TM), $E_0 \cos\theta$, components.

SSDI 0030-4018(94)00622-9

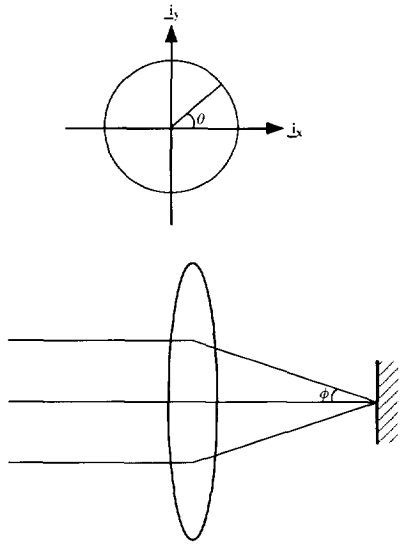

Fig. 1. The focussing geometry.

These components are then reflected from the specimen with appropriate amplitude Fresnel reflection coefficients, r_{TE} and r_{TM}, respectively. Upon further refraction by the lens we may resolve these fields back into i_x and i_y components and to write the field in the exit pupil of the lens as

$$\boldsymbol{E} = E_0 \begin{pmatrix} r_{TM} \cos^2\theta + r_{TE} \sin^2\theta \\ \frac{1}{2}(r_{TM} - r_{TE}) \sin 2\theta \end{pmatrix}, \tag{1}$$

where, r_{TE} and r_{TM} are evaluated at a particular value of ϕ which is related to the radial coordinate r via $r = f \sin\phi$ where f is the focal length of the lens for a lens obeying the sine condition [3]. We note that we have assumed that the (high aperture) objective lens itself does not influence the polarisation. We will return to this point later.

The intensity in the exit pupil is proportional to $|E|^2$ and may be written as

$$I \sim |r_{TM}|^2 \cos^2\theta + |r_{TE}|^2 \sin^2\theta, \tag{2}$$

which, in general, will not be angularly symmetric. The degree of asymmetry will depend upon both the specimen's complex refractive index, which determines the form of r_{TE} and r_{TM}, and the object lens numerical aperture which sets the upper limit on the angle of incidence, ϕ.

Eqs. (1) and (2) describe the field due to a plane polarized input wave. It is straightforward to extend the analysis to circular polarisation in which case the intensity in the exit pupil becomes

$$I \sim \tfrac{1}{2}(|r_{TM}|^2 + |r_{TE}|^2), \tag{3}$$

which shows no angular variation.

In order to quantify these effects for specimens of practical importance we constructed the system of Fig. 2. A 4-f lens waveguide system was used to image the exit pupil of the microscope objective lens onto a CCD array or a scanning pinhole detector. The relay lenses had a focal length of 20 cm and were 3 cm in diameter. A 600 μm pinhole was placed at the intermediate Fourier plane in order to remove any spurious reflections and stray light from other surfaces and parts of the optical system. The beamsplitter was oriented to be as normal to the signal beam as possible such that no polarisation dependent reflection effects were introduced.

Initially we elected to measure the intensity by scanning a 300 μm diameter pinhole across the image plane of the lens aperture, Fig. 2, in order to check the linearity and dynamic range of our CCD. In this case it proved to be more convenient to switch the input polarisation between i_x and i_y to obtain traces corresponding to $\theta = 0$ and $\theta = \pi/2$ in Eq. (2) rather than to rotate the pinhole scanning mechanism. In the case of circular polarisation the orientation of the diameter is not important since the intensity pattern shows no angular variation. Fig. 3 shows results for aluminium, silicon and glass substrates. The objective lens we used had a numerical aperture of 0.85 and hence an angular cut-off of 58.2° which is indicated by the dashed vertical line. The curves marked, x, correspond to $\theta = 0$ in Eq. (2) and hence are modelled by $|r_{TM}|^2$, the y-curves correspond to $|r_{TE}|^2$ whereas c denotes circular input polarisation which is modelled by Eq. (3). The values of complex

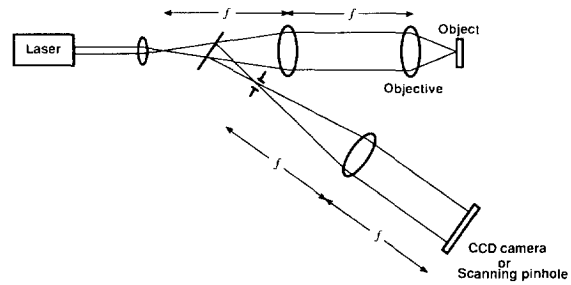

Fig. 2. The optical arrangement used to measure the intensity across the exit pupil of the objective lens.

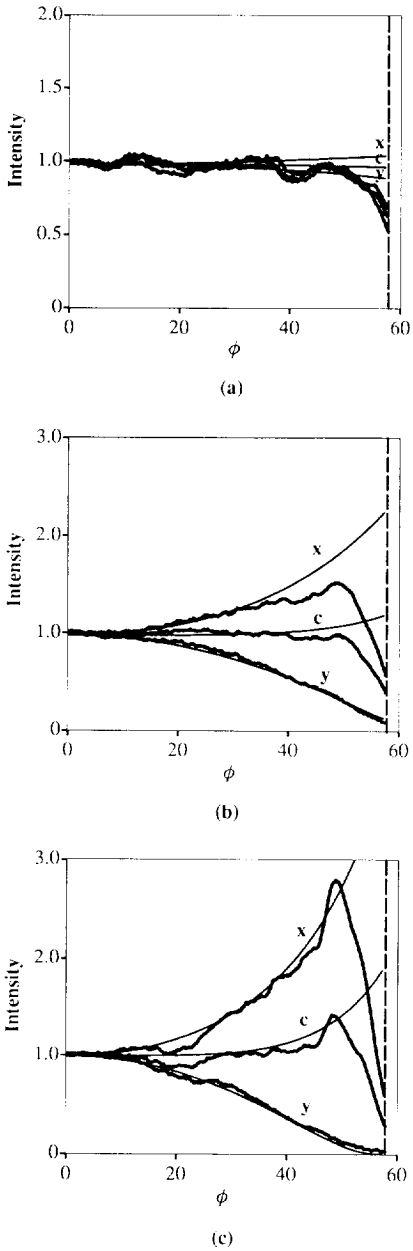

Fig. 3. Experimental and theoretical plots of the intensity in the exit pupil of the objective lens for a variety of substrates. The curves marked x and y correspond to $\theta=0$ and $\theta=\pi/2$ in Eq. (2) and Fig. 1, respectively. The curves labelled c correspond to circular polarized light. The curves are plotted as a function of angle ϕ up to the cut-off of 58.2° determined by the numerical aperture (0.85) of the objective lens. The results of using an aluminium specimen (a), silicon (b) and glass (c).

refractive index used in the Fresnel formulae to model these responses were $n=1.5$ (glass), $n=1.044$–i5.58 (aluminium) and $n=3.895$–i0.022 (silicon). The intensity axis was normalised to unity at $\phi=0$. The small oscillations of the measured results may well be due to speckle effects caused by the use of a laser source.

We note that we have presented the results by plotting the measured intensity as a function of the angle ϕ. In order to do this we calibrated the lens by measuring the angle ϕ when a thin pencil of light, travelling parallel to the optic axis was incident on the lens a distance h from the optic axis. For an objective lens obeying the sine condition the relationship between h and ϕ is given by [3]

$$h=f\sin\theta, \tag{4}$$

where f is the focal length. Fig. 4 shows the calibration of our 0.85 NA 50× Leitz lens together with the fit suggested by Eq. (4) for the case of $f=5$ mm. These results also confirm that our objective lens does indeed obey the sine condition.

It is clear that for aluminium, where $|r_{TE}|^2$ and $|r_{TM}|^2$ are not too different for the range of angles we have considered, there is very little difference between the x and y curves. This is not the case for either silicon or glass where we see at large values of ϕ, towards the edge of the objective, that the x and y curves are considerably different. Indeed the Brewster angle, 56°, is visible in the case of the glass substrate. In all cases the circular polarisation trace is relatively flat as might be expected since it essentially averages out the polarisa-

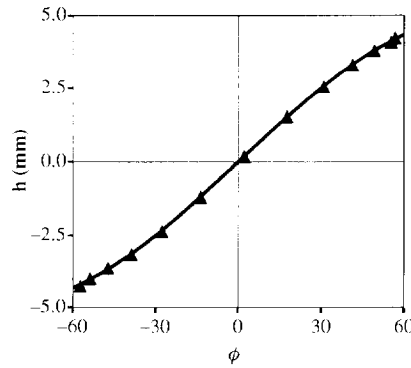

Fig. 4. The relationship between radial position on the objective lens and angle of incidence ϕ. The experimental data are shown as triangles. The theoretical fit (full line) also demonstrates that the objective lens obeys the sine condition.

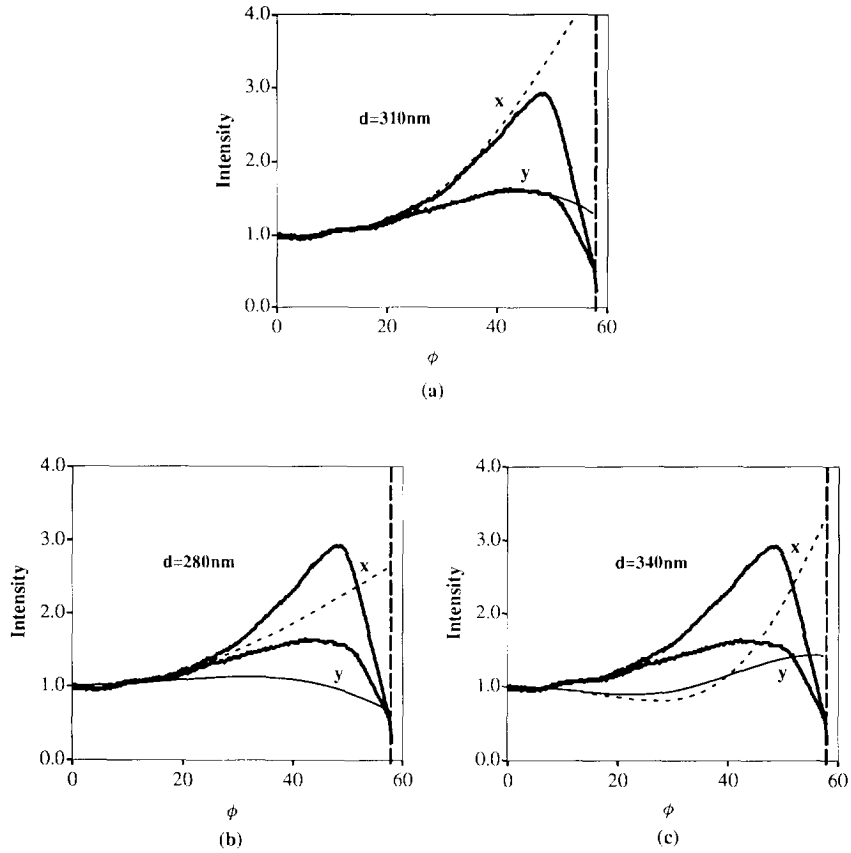

Fig. 5. (a) Experimental line scans across the full aperture of the 0.85 NA objective lens for the case of a silicon/silicon oxide specimen together with the theoretical curves corresponding to $d=310$ nm. (b) and (c) the dramatic effect of varying the oxide thickness by only 10% on the fit between experimental data and the theoretical curves.

tion effects. These results suggest that if we built a microscope where an image is formed by, for example, taking only the image corresponding to x ($\theta=0$) then it would show very different contrast to that corresponding to y ($\theta=\pi/2$) and that the difference would be material dependent. We shall return to this in the next section.

In order to further demonstrate the sensitivity of the method we took scans from a silicon specimen with an unknown thickness of silicon oxide on its surface. Fig. 5 shows the raw result together with attempts to model the behaviour by varying the thickness of the oxide layer where we assume a refractive index of 1.456 for the oxide layer. As we can see the fit is very sensitive to variations in the oxide thickness on the order of a few nm. We found that a thickness of $d=310$ nm gave the best fit. We have deliberately ignored the polarisation dependence of the transmission through the objective lens. This effect could be included by replacing r_{TE} by $K_{TE}^2 r_{TE}$ and r_{TM} by $K_{TE}^2 r_{TM}$ where K_{TE} and K_{TM} represent the transmission loss for the TE and TM polarisation, respectively [4]. These effects are greatest towards the edge of the lens where the light is most obliquely incident on the lens surfaces. Since it is impossible to know the precise form of these functions without detailed knowledge of the objective lens construction we have elected not to consider these effects and, as a consequence, our theory cannot be expected to fit the measured data perfectly at the extremities of the lens.

The results we have presented in Figs. 3 and 5 essentially confirm the prediction that the intensity along the diameter corresponding to TE polarisation increases and that along the diameter corresponding to TM polar-

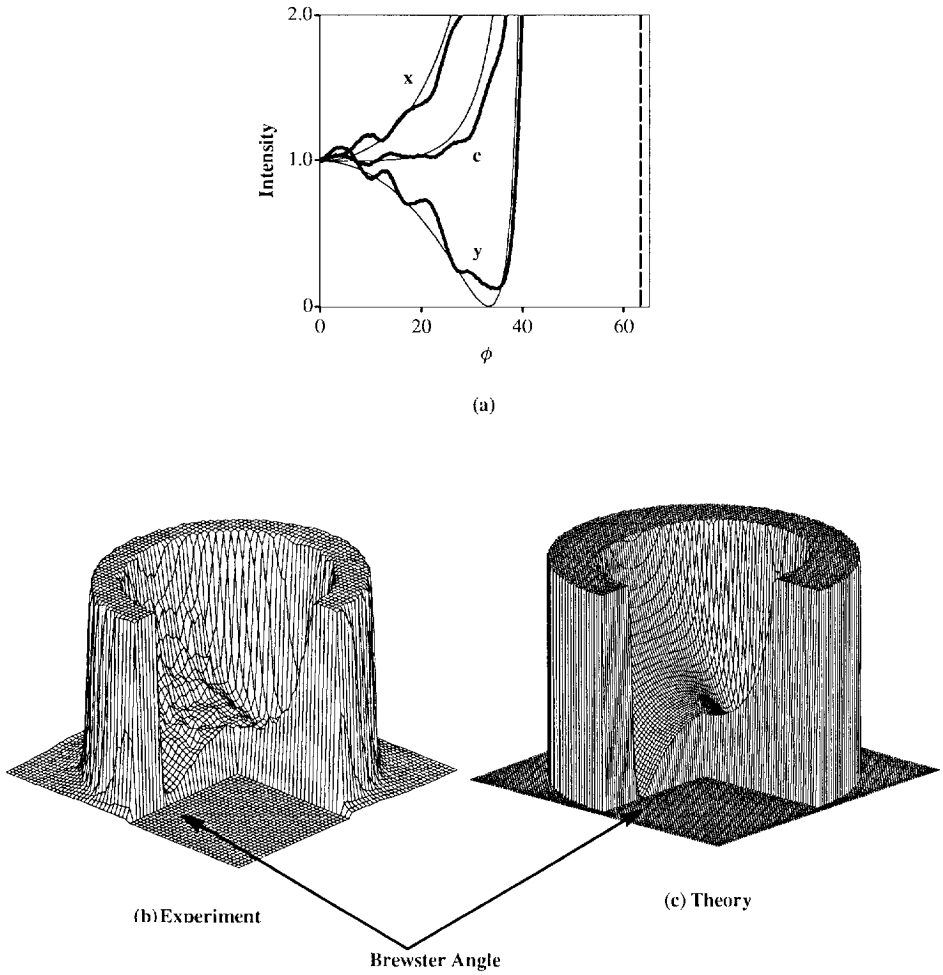

Fig. 6. (a) Experimental and theoretical line scans across the aperture of a 1.36 NA oil immersion lens. The specimen was essentially a glass/air interface. (b) Isometric data taken by a CCD camera and (c) the theoretical prediction. The isometric plots have been cut so as to reveal radii corresponding to TE and TM polarisation. The Brewster angle and critical angle are clearly visible.

isation decreases. The angular aperture of the objective is not large enough to demonstrate all the wealth of polarisation effects predicted by Eqs. (1) and (2). In order to do this we used a 1.36 NA oil immersion lens together with a glass cover slip. We focussed through the glass cover slip to the glass/air interface. If we assume the refractive index of the glass to be 1.5 then the Brewster angle is 33.7° and the critical angle, corresponding to total internal reflection, is 42°. These angles are well within the 64° aperture of our 1.36 NA immersion lens if we assume the index of the immersion oil to be 1.518. Fig. 6 shows the results. The theoretical and experimental isometric plots have been cut so as to reveal the diameters corresponding to TE and TM polarisations together with the region or total internal reflection. The full vertical scale is not shown since it would make visualising the TE/TM effects difficult.

3. Polarisation imaging

It is clear from our previous discussion that there is a wealth of specimen dependent information contained in the form of the optical field at the exit pupil of the objective lens. Indeed this is all the information that can be present in any final microscope image and the way in which this information is "compressed" into

the image depends crucially on the microscope imaging system.

The optical system of Fig. 2 could be turned into a scanning optical microscope very simply merely by introducing object scanning and replacing the CCD camera by a large area photodetector. If we assume that the optical field at this plane is essentially the same as the field at the exit pupil of the objective lens then the detected intensity will be proportional to the integral of Eq. (2) over the pupil of the lens if a plane polarised input beam is used. If the detector is uniform in sensitivity then we can see from Eq. (2) that when we perform the integral in θ,

$$\int_0^{2\pi} I \, d\theta = \tfrac{1}{2}(|r_{TM}|^2 + |r_{TE}|^2) \tag{5}$$

and hence the information contained in the angular distribution of the reflected field has been lost.

We may make similar remarks if a scanning confocal system is used which may be constructed simply by replacing the large 600 μm pinhole with a suitably small pinhole. In this case the detected signal is proportional to the modulus square of the integral of the optical field over the objective lens pupil [5]. This field is given by Eq. (1), from which we see

$$\int_0^{2\pi} \boldsymbol{E} \, d\theta = \frac{E_0}{2}\begin{pmatrix} r_{TM} + r_{TE} \\ 0 \end{pmatrix} \tag{6}$$

and again information contained within the angular distribution of the reflected field has been lost by averaging over the pupil. The contrast again depends only on r_{TE} and r_{TM} but the formal relationship is very different from that in the conventional microscope.

These observations, of course, explain why it is often difficult to observe polarisation dependent effects in conventional or confocal microscopes. If we revert to the conventional microscope we can overcome this problem by introducing a suitable mask in front of the photodetector which, in essence, limits the range of integration of θ. As an example if a slit were placed in front of the detector, aligned along the $\theta = 0$ direction, say, then the image signal I_1, would depend on $|r_{TM}|^2$ only. Similarly a slit oriented at right angles in the $\theta = \pi/2$ direction would give an image signal I_2 which would depend on $|r_{TE}|^2$ only. It would then be possible to form a composite image, $I_1 - I_2$, in which the image depended on the difference between $|r_{TM}|^2$ and $|r_{TE}|^2$ which is likely to be sensitive to the material properties of the specimen under examination.

In order to implement this difference imaging in a simple way we modified Fig. 2 as shown in Fig. 7 by introducing an electro-optic element to switch the input polarisation from $\boldsymbol{i}_x$ to $\boldsymbol{i}_y$. A single mask was placed in front of the detector which measured I_1 and I_2 as the input polarisation was switched by the electro-optic modulator.

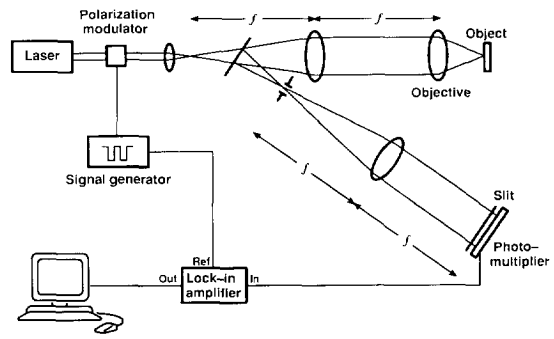

Fig. 7. Schematic diagram of the optical system used to obtain the difference images.

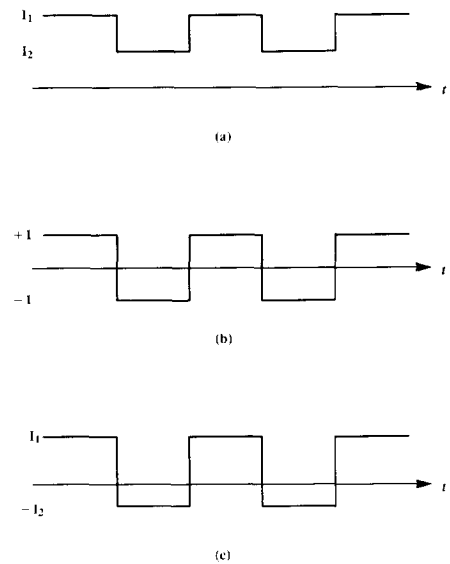

Fig. 8. Schematic explanation of the action of the lock-in detection scheme. (a) The switching of the detected signal between I_1 and I_2 as the electro-optic element switches the input polarisation due to the square wave modulation of (b). (c) The product of the waveforms of (a) (b) which reduces to a signal proportional to $I_1 - I_2$ when the waveform is time-averaged.

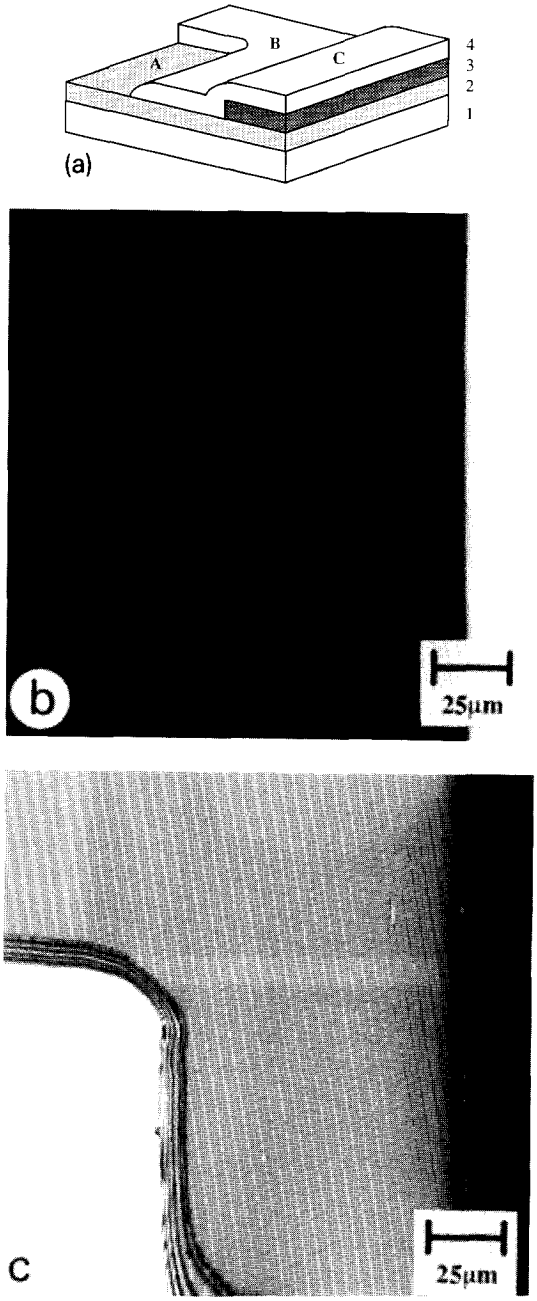

Fig. 9. (a) Schematic diagram of the specimen. Layer 1 refers to the silicon substrate. Layer 2 is a 500 nm thick SiO_2 film. Layer 3 represents a 100 nm gold deposit. Layer 4 represents a 1160 nm Si_3N_4 film. (b) Reflected Light image. (c) Polarisation difference image.

The difference image signal, $I_1 - I_2$, was obtained by the use of a lock-in amplifier whose action can be understood from Fig. 8. The electro-optic element was square wave modulated at 200 kHz and hence the photodetector output which was fed to the lock-in also switched between I_1 and I_2 at 200 kHz. The 200 kHz square wave modulation signal was also used as the reference signal to the lock-in amplifier. The action of the lock-in is to synchronously demodulate the input signal by multiplying it by the reference signal and then time averaging (low pass filtering). We see from Fig. 7 that the product switches between I_1 and $-I_2$ and hence the time averaged signal is be proportional to $I_1 - I_2$.

The specimen with which we chose to illustrate our technique was a microelectrode chip and is shown in Fig. 9a. It consists of a silicon substrate covered with a 500 nm thick layer of thermal silicon dioxide. The patterned layers consist of gold metallisation overlaid with 1160 nm of silicon nitride deposited by chemical vapour deposition. Fig. 9b shows a conventional scanning microscope image of the specimen taken with the system of Fig. 7 but without using the electro-optic modulator or the detector mask and taking the image signal directly from the photodetector output. The different regions of the specimen appear with the expected contrast.

Region C with the gold underlayer appears brightest whereas regions B and C appear dark. The difference between B and C however is not great. Indeed if we normalise the signals with respect to region C then the average signal in region B is 0.26 whereas in region A the value is 0.24.

Fig. 9c shows the difference image, $I_1 - I_2$, taken with the detector mask in place and the image signal derived from the output of the lock-in amplifier. A zero output signal is represented as mid-grey. The contrast is now dramatically different from that of Fig. 9b since it derives from differences in the reflection coefficients for TE and TM polarisation and not their absolute values.

Fig. 10 shows the intensity in the exit pupil – the conoscopic image – when the microscope is focussed on the regions A, B and C, respectively. The right hand column shows theoretical predictions generated by Eq. (2) together with the appropriate values of r_{TE} and r_{TM} [1]. The refractive index of Si_3N_4 was taken to be 2.16. Since I represents an integral along the horizontal axis of these results and I_2 represents an integral along the vertical axis it is to be expected that $(I_1 - I_2)$ will be

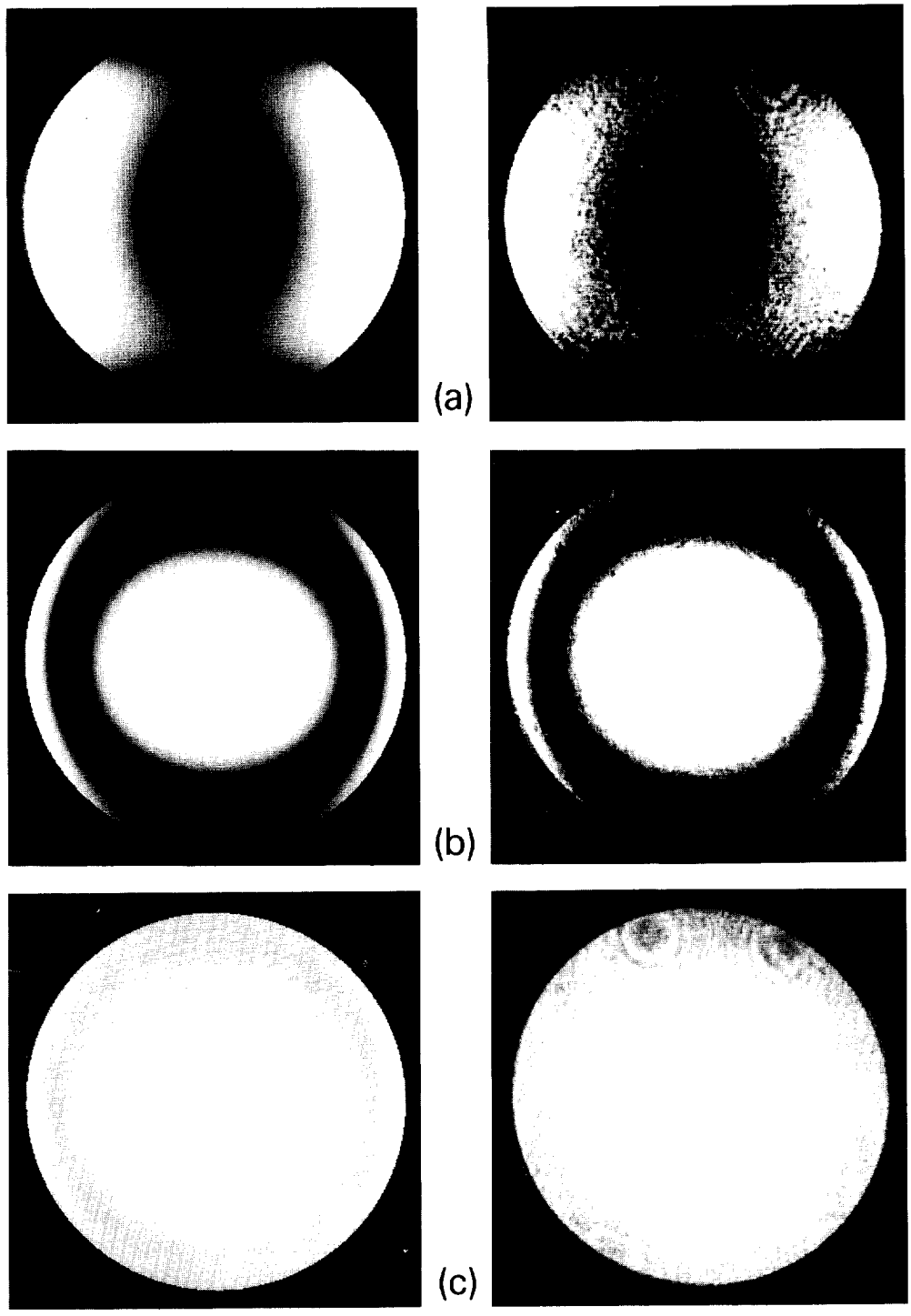

Fig. 10. Images of the exit pupil of the objective lens when focussed on different parts of the specimen. The left hand image is experimental and the right hand one the theoretical prediction; obtained by focussing on Si/SiO_2 region (a); on $Si/SiO_2/Si_3N_4$ region (b), and on $Si/SiO_2/Au/Si_3N_4$ (c).

greatest in region A, with an intermediate value in region B and the smallest difference in region C. These predictions are borne out in the image of Fig. 9c. The sensitivity of the technique to film thickness is also shown. The silicon nitride deposition was not well masked at the edge and this imperfection is seen very clearly in the fringing pattern in the polarisation difference image.

4. Conclusions

We have discussed the form of the optical field in the exit pupil of a high numerical aperture microscope objective when the lens is focussed onto an isotropic thin film specimen. The difference in the angular dependence of the reflection coefficient for TE and TM polarised light results in a non-circularly symmetric electric field which is particularly sensitive to the material properties of the specimen, and, in particular, film thickness. It is then a function of the particular microscope imaging system used which determines how this information is combined into a single image pixel value. The conventional microscope essentially performs an integral over the intensity in the exit pupil whereas the confocal system integrates over the exit pupil amplitude. In both cases the angular dependence information is lost.

In order to overcome this limitation we have proposed a polarisation contrast imaging technique in which image contrast depends, in essence, on the difference between the TE and TM reflection coefficients. However in order to obtain this polarisation contrast we have had to use a slit detector and so have traded spatial resolution for this enhanced contrast. This is fundamental to our method but the deterioration in resolution is not great.

Acknowledgements

We thank P.A. Leigh for providing the sample used to obtain Figs. 9 and 10. JBT and SVS would like to acknowledge financial support from the Rhodes Trust and the Royal Society respectively.

References

[1] R.M.A. Azzam and N.M. Bashara, Ellipsometry and polarised light (Elsevier, Amsterdam, 1989).
[2] M. Pluta, Advanced Light Microscopy, Vol. 3. Measuring Techniques (Elsevier, Amsterdam, 1993).
[3] M. Born and E. Wolf, Principles of optics (Pergamon, Oxford, 1975).
[4] H. Kubota and S. Inoué, J. Opt. Soc. Am. 49 (1959) 191.
[5] T. Wilson, ed., Confocal Microscopy (Academic Press, London, 1990).